Applied Surface Science 427 (2018) 1055–1064

Contents lists available at ScienceDirect

Applied Surface Science

journal homepage: www.elsevier.com/locate/apsusc

Full Length Article

Increase of porosity by combining semi-carbonization and KOH activation of formaldehyde resins to prepare high surface area carbons for supercapacitor applications

Ruben Heimböckel, Sebastian Kraas, Frank Hoffmann, Michael Fröba*

Department of Chemistry, Institute of Inorganic and Applied Chemistry, University of Hamburg, Martin-Luther-King Platz 6, D-20146 Hamburg, Germany

ARTICLE INFO

Article history:
Received 23 April 2017
Received in revised form 6 July 2017
Accepted 14 August 2017
Available online 24 August 2017

Keywords:
Phenol-formaldehyde resin
Supercapacitor
Activated carbon
KOH activation
Electrode material
Energy storage

ABSTRACT

A series of porous carbon samples were prepared by combining a semi-carbonization process of acidic polymerized phenol-formaldehyde resins and a following chemical activation with KOH used in different ratios to increase specific surface area, micropore content and pore sizes of the carbons which is favourable for supercapacitor applications. Samples were characterized by nitrogen physisorption, powder X-ray diffraction, Raman spectroscopy and scanning electron microscopy. The results show that the amount of KOH, combined with the semi-carbonization step had a remarkable effect on the specific surface area (up to S_{BET}: 3595 $m^2 g^{-1}$ and S_{DFT}: 2551 $m^2 g^{-1}$), pore volume (0.60–2.62 $cm^3 g^{-1}$) and pore sizes (up to 3.5 nm). The carbons were tested as electrode materials for electrochemical double layer capacitors (EDLC) in a two electrode setup with tetraethylammonium tetrafluoroborate in acetonitrile as electrolyte. The prepared carbon material with the largest surface area, pore volume and pore sizes exhibits a high specific capacitance of 145.1 F g^{-1} at a current density of 1 A g^{-1}. With a high specific energy of 31 W h kg^{-1} at a power density of 33028 W kg^{-1} and a short time relaxation constant of 0.29 s, the carbon showed high power capability as an EDLC electrode material.

1. Introduction

Electrochemical double layer capacitors (EDLC) also known as supercapacitors are electrochemical energy storage devices, which store and release energy by forming an electric double layer on the electrode surface. Ion ad- and desorption is a fast charge transport mechanism, therefore supercapacitors can be crucial elements in systems, where great amounts of energy have to be released quickly e.g. in combination with high energy batteries in electromobile applications [1–4]. Because of high power density, reversibility and long cycle life, supercapacitors are going to be a powerful competitor in many fields, such as hybrid vehicles. However, their specific energy is significantly lower than of conventional battery systems [5]. Therefore, increasing the specific energy is the main task of modern research regarding supercapacitors. The electrode material is a crucial element in the supercapacitor setup. Surface area, porosity, surface chemistry and conductivity of the electrode material determine the specific capacitance and therefore the specific energy density of the supercapacitor device. The voltage window is limited by the electrolyte and has little room for variation, especially for organic electrolytes. Many materials have been widely investigated such as porous carbons [6–9], conductive polymers [10] and metal oxides [11]. A lot of research was dedicated to porous carbons, such as activated carbons, which have a good electrical conductivity, possess great chemical stability, are of low cost, easily available and possess a high specific surface area. Therefore most commercial supercapacitors use biomass derived activated carbons like carbonized and activated coconut shell residues [12,13].

Depending on the organic precursor, the obtained activated carbons differ in surface area, pore sizes, pore volume and surface chemistry. The carbonization and activation process forms porous carbons by removing carbon atoms from the pore network and thus increasing the surface area, pore volume and average pore size. Tailoring of specific surface area and pore sizes of the carbon electrodes is desired. A high specific surface area increases the specific capacitance although this effect is limited [1]. Micropores (<2 nm) can increase the specific capacitance, when their size matches the size of electrolyte ions. By distorting the solvation shell of the electrolyte ions, the thickness of the double layer is reduced, which increases the specific capacitance [14]. However, small micropores limit the accessibility to electrolytes during the charge/discharge process. The ion diffusion within small micropores, especially at large cur-

* Corresponding author.
E-mail address: froeba@chemie.uni-hamburg.de (M. Fröba).

http://dx.doi.org/10.1016/j.apsusc.2017.08.095
0169-4332/

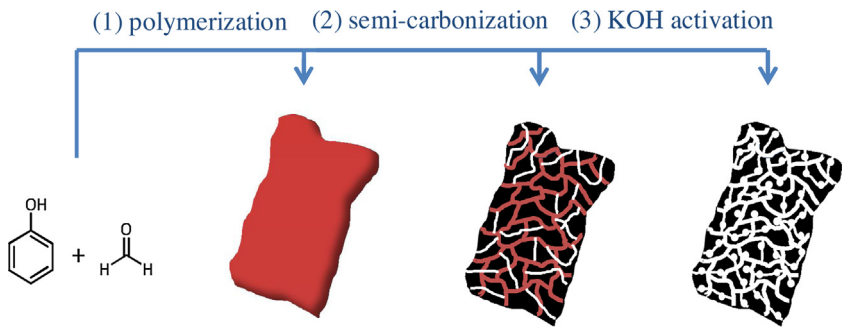

Fig. 1. Synthesis scheme for the preparation HSAC from PF resins. (1) polymerization of the PF resin under strong acidic conditions; (2) semi-carbonization of the PF resins at 500 °C under argon atmosphere; chemical activation of the semi-carbonized carbons with different ratios of KOH at 900 °C under nitrogen atmosphere.

rent densities is limited as well. Therefore interconnected small mesopores are favourable to enhance ion diffusion with a high speed at a high loading current density and the efficient utilization of specific surface areas [15].

Phenolic formaldehyde (PF) resins are widely used organic precursors for generating carbon materials, like ordered mesoporous carbons and carbon aerogels [16–18]. There were also many attempts to use carbons based on chemically or physically activated formaldehyde resins for supercapacitor electrodes [19–25]. The degree of polymerization of PF resins can be controlled very well. By varying the reaction conditions, e.g. acid or alkaline catalysis or different phenol/formaldehyde ratios, novolacs or more crosslinked resols can be obtained [26]. By use of a soft templating method a mesoporous PF resin can be formed leading to carbons with defined mesopores. As pore-directing template triblock copolymers are used [27–30]. Another possible approach to create small mesopores is via chemical activation of carbons without the use of any structure directing agents [20,31]. Chemical activation of ordered mesoporous carbons is very likely to increase the specific surface area of the carbons, but the ordered mesoporous structure is strongly damaged [32]. Recent studies showed that PF based carbons synthesized under acidic conditions possessed an exceptional resistance to a wide range of activation agents and activation temperatures [33–35]. The preservation of ordered mesopores with respect to chemical KOH activation was found to be temperature dependent. When ordered mesoporous carbons experience an activation at 700 °C or higher, the carbons still keep most of the ordered mesoporous structure [36]. The pyrolysis temperature prior to the activation is crucial for the chemical and thermal stability of the carbons. It strongly affects the structure of the carbons and therefore the preservation of the ordered mesoporous structure against chemical activation. With a higher carbonization temperature the carbonaceous framework has a more rigid structure, which can withstand KOH activation processes for a possible preservation of ordered pore structures [37]. Then again, a lower semi-carbonization temperature prior to the activation can make the pore creating activation procedure more effective due to the less rigid structure of the carbonaceous framework [38–41].

Here we report about a facile method to prepare high surface area activated carbons (HSAC) with interconnected micro- and mesopores. As seen in Fig. 1. PF resins were synthesized under strong acid conditions, to obtain a rigid polymer network. The polymers were then semi-carbonized and activated with different amounts of KOH, to obtain highly porous carbons. No structure directing agents were used during the synthesis. We chose acid conditions during the polymerization step to obtain a stable polymer network on one hand, and combine it with a semi-carbonization temperature of 500 °C on the other hand to synthesize carbons with modest resistance against chemical activation. Thus a variety of KOH ratios can be used. For comparison purpose one carbon sample was not activated after semi carbonization at 500 °C (HSAC-0). Another carbon sample was carbonized at 900 °C (HSAC-5-nSC) prior to chemical activation, to show the effect of chemical activation with a combined semi-carbonization process to obtain carbons with very high surface areas. Electrochemical tests were performed using electrodes of the prepared carbons. With organic electrolytes, cyclic voltammetry, galvanostatic charge/discharge tests and electrochemical impedance spectroscopy were performed to investigate the potential of the HSAC as supercapacitor electrodes.

2. Materials and methods

2.1. Materials synthesis

In a typical synthesis of HSAC 2.2 g phenol (ABCR) was dissolved in 30 g ethanol. While stirring, 4.4 mL of formaldehyde (Grüssing, 37 wt.% in water) solution and 10 mL of hydrochloric acid (HCl, 37 wt.%) were added. The mixture was heated to 95 °C for 24 h. The bright brown PF resin was filtered, washed with ethanol and dried for 12 h at 100 °C. The obtained pulverulent dark red polymer was then heated in a quartz tube furnace at 500 °C for 3 h under argon inert gas atmosphere with a heating rate of 5 °C min^{-1}. The semi-carbonized material was mixed with different mass ratios of potassium hydroxide (1, 2.5, 5 and 8) and dissolved in water and ethanol. The mixture was then dried at 100 °C for 24 h to ensure a good amalgamation of the semi-carbonized carbon and potassium hydroxide. The carbon/KOH mixture was activated at 900 °C with no holding time under nitrogen gas atmosphere. The resulting product was washed with diluted HCl and distilled water to remove any impurities until the filtrate was pH neutral. The product was dried for 24 h at 100 °C. The prepared samples are named HSAC-0, HSAC-1, HSAC-2.5, HSAC-5 and HSAC-8 depending on the mass ratios of KOH to carbon. For HSAC-5-nSC the phenol-formaldehyde resin was carbonized in a quartz tube furnace at 900 °C for 3 h under argon inert gas atmosphere. The carbon was mixed with KOH in a mass ratio of 5 to 1 and then activated at 900 °C under nitrogen gas atmosphere with no holding time. The resulting product was washed with diluted HCl and distilled water until the filtrate was pH neutral prior to drying at 100 °C for 24 h.

2.2. Material characterization

Nitrogen (N_2) adsorption-desorption isotherms were performed on a Quadrasorp SI-MP analyser from Quantachrome at 77 K. The pore size distributions, pore volume and surface area were calculated by QSDFT method for nitrogen using the slit pore equilibrium kernel for nitrogen at carbon. The micropore volume was collected from the cumulative pore volume at 2 nm calculated by QSDFT method. The surface area was also calculated using the BET (Brunauer-Emmet-Teller) method. A relative pressure range of

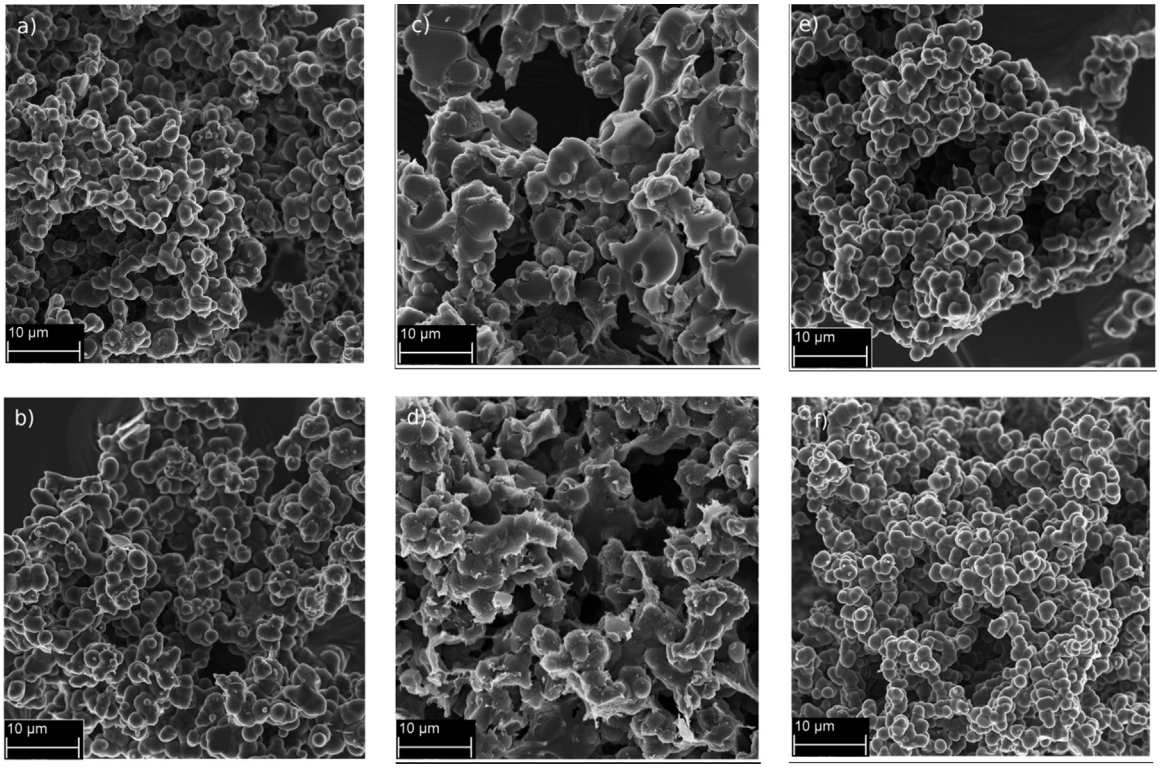

Fig. 2. SEM images of the activated carbons (a) HSAC-1, (b) HSAC-2.5, (c) HSAC-5, (d) HSAC-8, (e) HSAC-5-nSC and (f) HSAC-0.

0.05–0.3 was selected to ensure that a positive line intersect of multipoint BET fitting ($C > 0$) was obtained and $V_{ads}(1 - P/P_0)$ increased with P/P_0 [42,43]. X-ray diffraction patterns were obtained on a Panalytical X'Pert Pro (Cu Kα radiation) in reflection mode. Raman spectra were recorded on a SENTERRA microscope from Bruker. The source of radiation was a laser operating at a wavelength of 633 nm. SEM images were taken on NTS LEO-1525 from Carl Zeiss Company.

2.3. Electrochemical characterization

Electrodes were prepared by mixing 70 wt.% of active material with 20 wt.% of polyvinylidene fluoride (PVDF) binder (Sigma-Aldrich, 10% suspension in *N*-methyl-pyrrolidone, NMP) and 10 wt.% VULCAN XC72R (CABOT) as conductive additive in a slurry with NMP. The slurry was coated on aluminium foil (Custom Cells, 15 µm) and dried at 100 °C in vacuo. The thickness of the electrodes of each sample is about 65 µm (including Al foil). Electrodes were cut out with a diameter of 1.8 cm with mass loadings from 0.60 to 1.07 mg cm^{-2} of total active carbon material. The electrochemical measurements were performed in a two-electrode test cell setup (El-Cell) using stainless steel electrodes (1.8 cm diameter). Symmetrical electrochemical capacitors were built using two carbon electrodes of identically mass, electrically isolated by glassy fibrous separator (Whatman, 50 µm). A 1 M tetraethylammonium tetrafluoroborate ($TEABF_4$, electrochemical grade, Sigma-Aldrich) solution in acetonitrile (AN, 99.999%, Sigma-Aldrich) was used as electrolyte. The electrochemical characterization was performed using a computer-controlled potentiostat (Biologic VMP3). Before electrochemical tests were carried out, each test cell was cycled at a scan rate of 75 mV s^{-1} for 25 times to ensure wettability the electrolyte and equilibrium state of electrolyte ions on the carbon electrode surface. All calculations regarding electrochemical tests were calculated by the means of the following formulas (1)–(6) [7,44,45].

Cyclic voltammetry (CV) was conducted between 0 and 2.5 V at increasing scan rates from 10 to 2500 mV s^{-1}. The specific capacitance of both electrodes was calculated from the area of the voltammograms by means of the following formula:

$$C_{CV} = \frac{4\int IdV}{\nu m \Delta V} \quad (1)$$

where I is the current (mA), ν the scan rate (mV s^{-1}), ΔV the voltage window (V), and m the mass (g) of total active carbon material of both electrodes.

Galvanostatic charge/discharge cycling was also performed in the 0–2.5 V range at current densities ranged between 1 and 20 A g^{-1}, based on the total electrode mass of both electrodes. The specific capacitance of both electrodes determined from galvanostatic cycles was calculated by means of the formula:

$$C_{DC} = \frac{2I}{(dV/dt)m} \quad (2)$$

where dV/dt is the slope of the discharge curve (V s^{-1}).

Electrochemical impedance spectroscopy (EIS) was carried out at open circuit voltage within the frequency range of 10 mHz to 500 kHz and a 5 mV AC amplitude. Plots of the dependence of the capacitance on the frequency were recorded to characterize the impedance of the samples. The real specific capacitance of both electrodes C'_{EIS} was calculated according to the following formula and normalized with respect to the specific capacitance at 10 mHz:

$$C'_{EIS} = \frac{4|Im(Z)|}{2\pi f |Z|^2 m} \quad (3)$$

where f is the operating frequency (Hz), Im(Z) the imaginary component of the impedance (Ohm) and Z the total impedance (Ohm). The imaginary specific capacitance of both electrodes C''_{EIS} was cal-

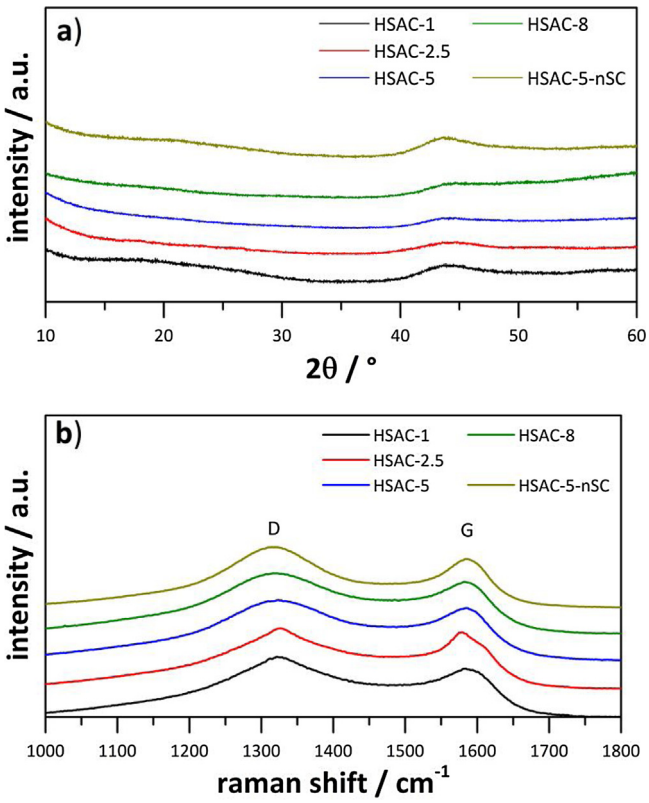

Fig. 3. p-XRD patterns (a) and Raman spectra (b) of the activated carbon materials.

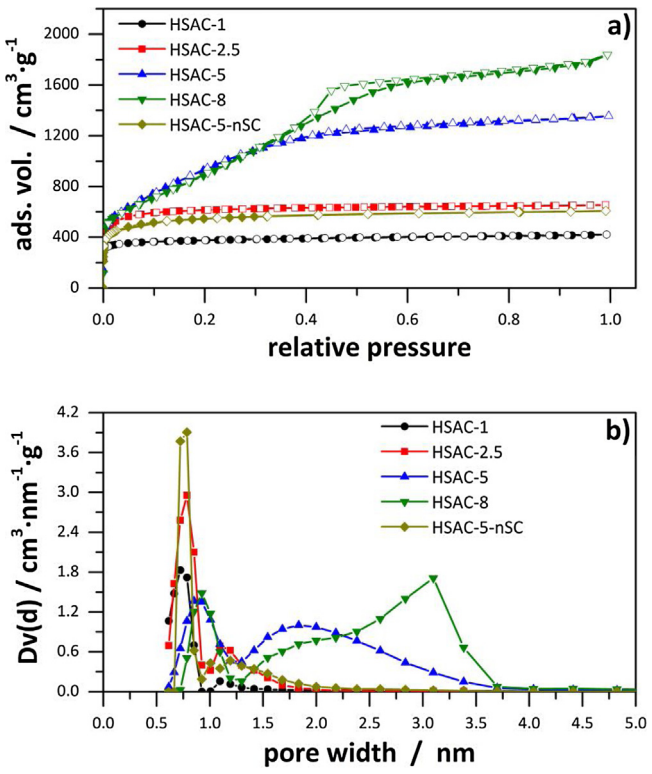

Fig. 4. (a) N_2 adsorption-desorption isotherms (77 K) of the carbon materials; (b) pore size distributions calculated by the QSDFT method.

culated by means of following formula and normalized with respect to the highest imaginary specific capacitance:

$$C''_{EIS} = \frac{4|\mathrm{Re}(Z)|}{2\pi f|Z|^2 m} \quad (4)$$

where Re(Z) is the real part of the impedance (Ohm). The time relaxation constant τ_0, which separates the capacitive behaviour and the resistive behaviour of the supercapacitor, was deduced from the frequency f_0 as follows: $\tau_0 = 1/f_0$, where f_0 is the peak frequency of the plot from the imaginary capacitance.

The specific energy (Wh kg^{-1}) was calculated using the following formula:

$$E = \frac{1}{8} C_{DC} \Delta V_d^2 \quad (5)$$

where C_{DC} is the gravimetric specific capacitance (F g^{-1}) obtained from the galvanostatic discharge and ΔV_d the operating voltage window ($V_{max} - IR_{drop}$). The specific power (W kg^{-1}) was calculated according to the formula:

$$P = \frac{E}{t_d} \quad (6)$$

where t_d is the discharge time.

3. Results and discussion

3.1. Material characterization

The prepared HSAC were characterized by scanning electron microscopy and the images of HSAC-1 and HSAC-2.5 are given in Fig. 2a and b. It can be seen that HSAC-1 and HSAC-2.5 present a nanonetwork structure which is composed of spherical carbon nanoparticles, similar to the control sample HSAC-0 (Fig. 2e) and typical for carbons, based on formaldehyde resins [46]. The loose aggregation of the spherical carbon nanoparticles leads to a formation of cavities within the nanonetwork which are 2–10 μm in diameter. The nanonetwork structures of HSAC-5 and HSAC-8 possess the same cavities as HSAC-0, HSAC-1 and HSAC-2.5. However, a change in structure can be observed as the spherical particles agglomerated strongly, which is clearly caused by the increasing KOH/carbon ratio. Such an altering of the structure is unusual for carbons based on formaldehyde resins [47]. Due to the low semi-carbonization temperature prior to the chemical activation the nanonetwork is less rigid, which leads to a stronger agglomeration of the spherical particles after the chemical activation with an increasing KOH/carbon ratio [36]. Fig. 2e shows that the nanonetwork of HSAC-5-nSC is composed loose aggregated spherical particles which form cavities in the network, similar to HSAC-0. HSAC-1 and HSAC-2.5. The nanonetwork withstood an altering by KOH activation despite the high KOH/carbon ration of 5. This is the effect of the higher carbonization temperature prior to KOH activation which led to a more rigid carbon nanonetwork and the preservation of the loose aggregated spherical particles [37].

To investigate the composition of the HSAC, powder X-ray diffraction (p-XRD) analysis was performed (Fig. 3a). All carbon p-XRD pattern show weak and extremely broad reflections at 44.0° (2θ) corresponding to (101) diffractions of a turbostratic carbon structure [48]. The absence of (002) diffractions for all HSAC indicates a rotationally disordered structure of carbon layers, emphasizing the turbostratic carbon structure. The Raman spectra (Fig. 3b) showed two broad peaks around 1320 cm^{-1} and 1585 cm^{-1} corresponding to the D (disordered carbon) and the G-band (ordered graphitic lattice) respectively, which are typical of carbonaceous materials [49,50]. The calculated I_D/I_G ratios, which reflect the graphitic degree of the carbon materials, are in the range of 1.07 (HSAC-2.5) to 1.25 (HSAC-5-nSC) showing rather a low degree of graphitization (Table S1). Results from p-XRD and Raman scattering indicate that the HSAC are amorphous materials. This

Table 1
N_2 physisorption derived data of the HSAC.

Sample	S_{BET}/m² g⁻¹	S_{DFT}/m² g⁻¹	V_t/cm³ g⁻¹	V_{mic}/cm³ g⁻¹
HSAC-0	483	574	0.19	0.18
HSAC-1	1473	1583	0.60	0.54
HSAC-2.5	2383	2108	0.93	0.91
HSAC-5	3537	2480	1.96	0.97
HSAC-8	3595	2551	2.62	0.86
HSAC-5-nSC	2068	1811	0.86	0.80

S_{BET}: BET surface area; S_{DFT}: QSDFT surface area; V_t: total pore volume; V_{mic}: micropore pore volume.

Table 2
Electrochemical properties of the EDLC prepared from the HSAC in 1 M $TEABF_4$/AN.

Sample	C_{CV}/F g⁻¹	C_{CDC}/F g⁻¹	R_{ESR}/Ω	τ_0/s
HSAC-1	15.4	6.9	0.65	>100
HSAC-2.5	96.7	117.1	0.65	1.19
HSAC-5	123.6	142.0	0.68	0.75
HSAC-8	136.2	145.1	0.48	0.29
HSAC-5-nSC	81.4	89.5	0.72	1.50

C_{CV}: specific capacitance (cyclic voltammetry at 10 mV s⁻¹); C_{CDC}: specific capacitance (galvanostatic discharge) at 1 A g⁻¹; R_{ESR}: equivalent series resistance; τ_0: time relaxation constant.

can be attributed to the low semi-carbonization temperature leading to a low degree of graphitization. For the formation and parallel stacking of graphitic layers, temperatures of 2000 °C and higher are required. Additionally, the KOH activation lowers the degree of graphitization drastically, by increasing porosity and generating structural defects, as well as doping of oxygen leading to oxygen containing functional groups at the surface of the carbon materials [51,52].

The prepared HSAC were characterized with N_2 physisorption (77 K), to investigate their porosity. The corresponding isotherms can be seen in Fig. 4a and the N_2 physisorption derived data are summarized in Table 1. HSAC-1 and HSAC-2.5 show a typical type I isotherm, indicating carbon materials with predominantly micropores. The isotherms of HSAC-5 and HSAC-8 show a slope at relative pressures from 0.1 to 0.4 resulting from widening of pores and broad pore size distributions of large micropores and mesopores [42]. HSAC-5-nSC on the other hand shows a type I isotherm for microporous carbon, indicating that the KOH activation is less effective in generating larger pores, compared to HSAC-5. All prepared HSAC have micropores from 0.62 to 1.10 nm originating from the carbonization processes and additionally from the etching of carbon during the KOH activation (Fig. 4b). Additionally to micropores, HSAC-5 and HSAC-8 have also mesopores up to 3.5 nm, while HSAC-8 has slightly larger pore sizes than HSAC-5. It is clear, that a higher KOH/carbon ratio leads to an enlargement of the pores and a broader pore size distribution. HSAC-5-nSC however has significantly smaller pores than HSAC-5 despite the same KOH ratio for the chemical activation. This shows the formation of a more rigid carbonaceous framework due to carbonization at 900 °C of the polymer precursors, prior to KOH activation. The prepared HSAC possess high values for BET surface areas ranging from 1473 to 3595 m² g⁻¹ (Table 1). It is known, that the BET method overestimates the surface area for microporous carbons with pore sizes greater than 0.9 nm [53,54]. Therefore the DFT surface area is was obtained additionally (Table 1). As expected, the highest DFT surface area is 2551 m² g⁻¹ and smaller than the corresponding BET surface area. Nevertheless, the surface area directly depends on the KOH/carbon ratio with HSAC-1 having the smallest and HSAC-8 the highest surface area. The same can be seen for total pore volumes (V_t). With an ultra-high pore volume of 2.62 cm³ g⁻¹ HSAC-8 has the highest total pore volume among the HSAC, while HSAC-1 has the lowest total pore volume with 0.60 cm³ g⁻¹. The micropore volume increases with the amount of potassium hydroxide used for chemical activation from 0.54 to 0.97 cm³ g⁻¹ and then decreases to 0.86 cm³ g⁻¹ with HSAC-5 having the highest micropore volume. The chemical activation generates new micropores predominantly, but with a higher amount of chemical activation agent the newly formed micropores become larger, hence forming small mesopores and lowering the micropore volume. The specific surface area, total pore volume and micropore volume of HSAC-5 are significantly larger than of HSAC-5-nSC as seen in Table 1. In fact the material properties of HSAC-5-nSC are similar to HSAC-2.5 despite the use of twice as much KOH. This emphasizes the greater effectiveness of the chemical activation combined with a semi-carbonization prior to the activation. HSAC-0 is purely microporous carbon with the lowest surface area, pore sizes and total pore volume (Fig. S1).

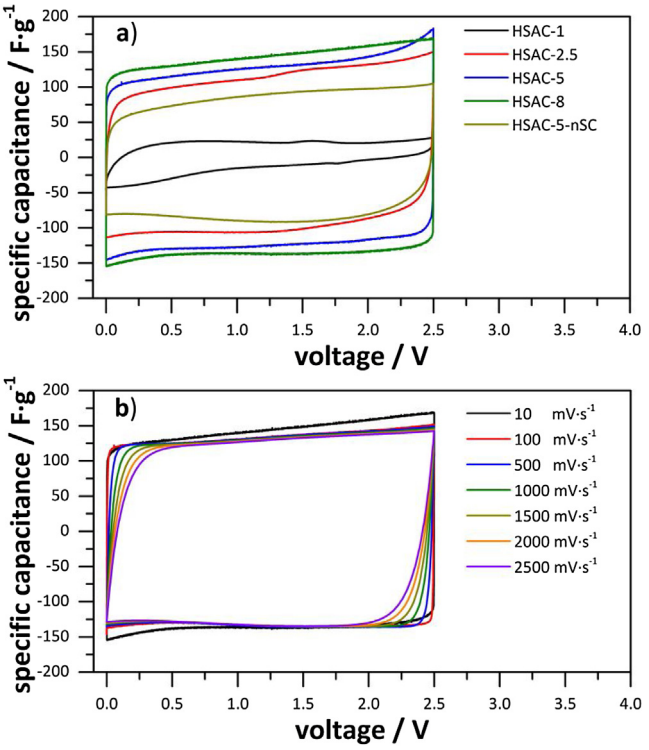

Fig. 5. (a) Cyclic voltammograms of HSAC at 10 mV s⁻¹ in 1 M $TEABF_4$/AN; (b) cyclic voltammograms of HSAC-8 at different scan rates.

3.2. Electrochemical characterization

The prepared symmetric EDLC were firstly characterized with cyclic voltammetry and the results a summarized in Table 2. The CV of the carbons at a scan rate of 10 mV s⁻¹ show typical rectangular shapes which proves well developed electrochemical double layer capacitance properties (Fig. 5a). Furthermore, a small increase in capacitance with increasing cell potential can be observed. This can be attributed to the non-metallic nature of carbon, where more charges can be accumulated as the density of states of charge carriers changes during increase of applied potential [55–57]. While the specific capacitance of HSAC-1 with 15.4 F g⁻¹ is quiet low, the specific capacities of HSAC-2.5, HSAC-5, HSAC-8 and HSAC-5-nSC are higher with 96.7, 123.6, 136.2 and 81.4 F g⁻¹ respectively. This can be attributed to the larger specific surface areas, which grant superior access for electrolyte ions to the interconnected pore system and therefore more electrolyte ions form electric double layers at the electrode surface [23]. Noticeably the CV curves of HSAC-5 and HSAC-8 show only small distortions. As can be seen for HSAC-8 in Fig. 5b even at a very high scan rate of 2500 mV s⁻¹ the overall electrochemical performance is excellent showing a rectangular shape

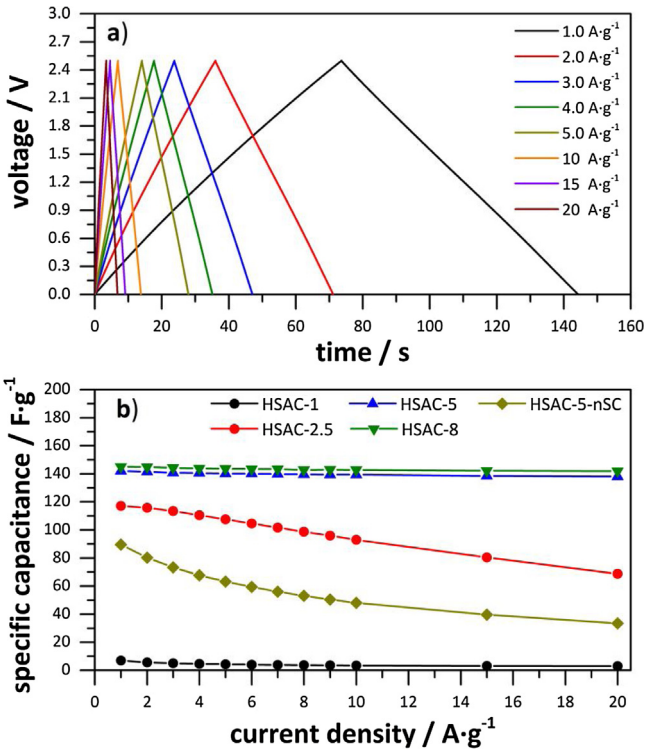

Fig. 6. (a) Galvanostatic charge/discharge profile of HSAC-8 at different current densities; (b) specific capacitance of HSAC as a function of discharge current density.

with minor distortions only. Additionally, almost no loss in capacitance can be observed. This indicates a very rapid current response on voltage reversal and ultra-fast ion-diffusion kinetic in the carbon framework. Similar excellent current response can be observed for HSAC-5 (Fig. S2c). Next to the high surface area and pore volume HSAC-5 and HSAC-8 contain a higher amount of mesopores which contribute the fast ion-diffusion within the carbon pore network, leading to high power retention.

The electrochemical behaviour was further investigated with galvanostatic charge/discharge tests. For all current densities from 1 to 20 A g^{-1} the galvanostatic charge/discharge results from HSAC-8 (Fig. 6a) show symmetrical and linear shapes supporting the CV observations of the ideal double layer behaviour. The specific capacitance of HSAC-8 and HSAC-5 stand out with values as high as 145.1 F g^{-1} and 142.0 F g^{-1} respectively, at a current density of 1 A g^{-1}. The specific capacitance compare very well with that of various state-of-the-art porous carbon materials and phenolic resin based carbon materials used as electrode materials for capacitors with organic electrolytes [21,22,58,59,45,60,61]. A detailed comparison with formaldehyde resin based carbon materials is given with Table S2. Both HSAC-8 and HSAC-5 have a very high specific surface area around 2500 m^2 g^{-1} (DFT) which give the main contribution to the high specific capacitance. While the micropore volume of HSAC-5 (0.97 cm^3 g^{-1}) is higher than of HSAC-8 (0.86 cm^3 g^{-1}) their highest specific capacitance calculated form galvanostatic discharge is similar. On the one hand, the capacitance of HSAC-5 should be higher than of HSAC-8 due to a possible increase of capacitance of micropores below and around 1 nm [14,57]. On the other hand, HSAC-8 has a very high pore volume (2.62 cm^3 g^{-1}) due to larger pore sizes and a higher content of mesopores, which can increase the capacitive behaviour [60]. While it is typical for EDLC to experience a significant deterioration of capacitance at higher current densities due to diffusion limitations of electrolyte ions, the loss of capacitance with respect to higher current densities for HSAC-8 is as small as 2.2%, still having a capacitance of 141.8 F g^{-1} at a high current density of 20 A g^{-1} originating from rapid ion transport within the pore network (Fig. 6b). The same can be observed for HSAC-5 having a loss in capacitance of only 2.7% and a high specific capacitance of 138.1 F g^{-1} at a current density of 20 A g^{-1}. Such performances make HSAC-5 and HSAC-8 good candidates for high power electrochemical applications [3,44]. HSAC-2.5 possesses a high specific capacitance of 117.1 F g^{-1} at 1 A g^{-1}, but the capacitance decreases significantly at higher current densities. The specific capacitance from HSAC-5-nSC is as high as 89.5 F g^{-1} but lower than the specific capacitance of HSAC-2.5 due to the lower content of micropores. With respect to higher current densities the specific capacitance decreases as well. The overall capacitive performance of HSAC-1 is rather poor due to low specific surface area, pore volume and small pores. It is clear, that high specific surface area, large pore volume and high content of micropores are crucial for obtaining high capacities, while mesopores are important for fast ion transport in the pore network leading to high capacitance values even at high current densities [62].

EIS was carried out between 500 kHz and 10 mHz for further investigation of the prepared EDLC. Results are usually plotted in a Nyquist plot, in which the intersection of the real impedance shows the equivalent serial resistance (R_{ESR}) at high frequencies. It reflects the bulk resistance of the electrolyte, contact resistance of electrode material and current collector as well as intrinsic resistance of the carbon electrode. A semicircle in mid to higher frequency region up to 50 Hz, reflects the charge transfer resistance from faradaic charge transfers and charge accumulation of electrolyte ions on the electrode surface [63]. In addition the Warburg resistance, a short 45° segment at mid frequencies to 5 Hz, is related to the diffusion resistance of the electrolytes within the pore network. At low frequencies a straight line with a large slope shows ideal double layer behaviour. As seen in the Nyquist plot of the HSAC in Fig. 7a the R_{ESR} values for all investigated carbons are very low, between 0.48 Ω (HSAC-8) and 0.72 Ω (HSAC-5-nSC), which indicates a sufficient intrinsic conductivity for electrochemical purpose [64]. The investigate carbons show either no significant semicircle or a short semicircle, like HSAC-5-nSC, indicating mainly electrochemical double layer energy storage for the prepared systems. The Warburg segments are of short length for all HSAC pointing to low diffusion resistance for short diffusion ways in the pore network in general. In Fig. 7b the phase angles as a function of the frequency for all samples are shown. For perfect double layers, the phase angle is very close to −90°. The samples HSAC-8 and HSAC-5 show almost perfect double layer behaviour with phase angles of −88.2° and −88.4°, attributed to the mesopores which enhance electrolyte ion migration within the whole carbon framework. Interestingly the phase angle of the microporous HSAC-2.5 and HSAC-5-nSC is −85.9° and −85.5° respectively indicating that large micropores enhance electrolyte migration likewise at low frequencies. That was observed for microporous carbide-derived carbons as well [9,65]. HSAC-1 shows rather poor capacitive behaviour at low frequencies due to the supermicropores which prohibit resistance free migration within the pore network.

Fig. 7c shows the normalized real capacitance dependent on the frequency. For the HSAC the frequency response of the capacitance depends on the pore sizes. It is clear that with increasing frequency the capacitance decreases due to diffusion limitations of electrolyte ions. While HSAC-8 shows superior characteristics by having almost the same capacitance at a relatively high frequency of 1 Hz, the capacitance of HSAC-1 decreases already at 10 mHz. From the imaginary resistance plotted against the frequency, the time relaxation constant τ_0 can be calculated by $\tau_0 = 1/f_0$ given by the maximum of the normalized imaginary resistance at the frequency f_0. (Fig. 7d). The time relaxation constant states the discharge time of a capacitor in which the device energy efficiency is

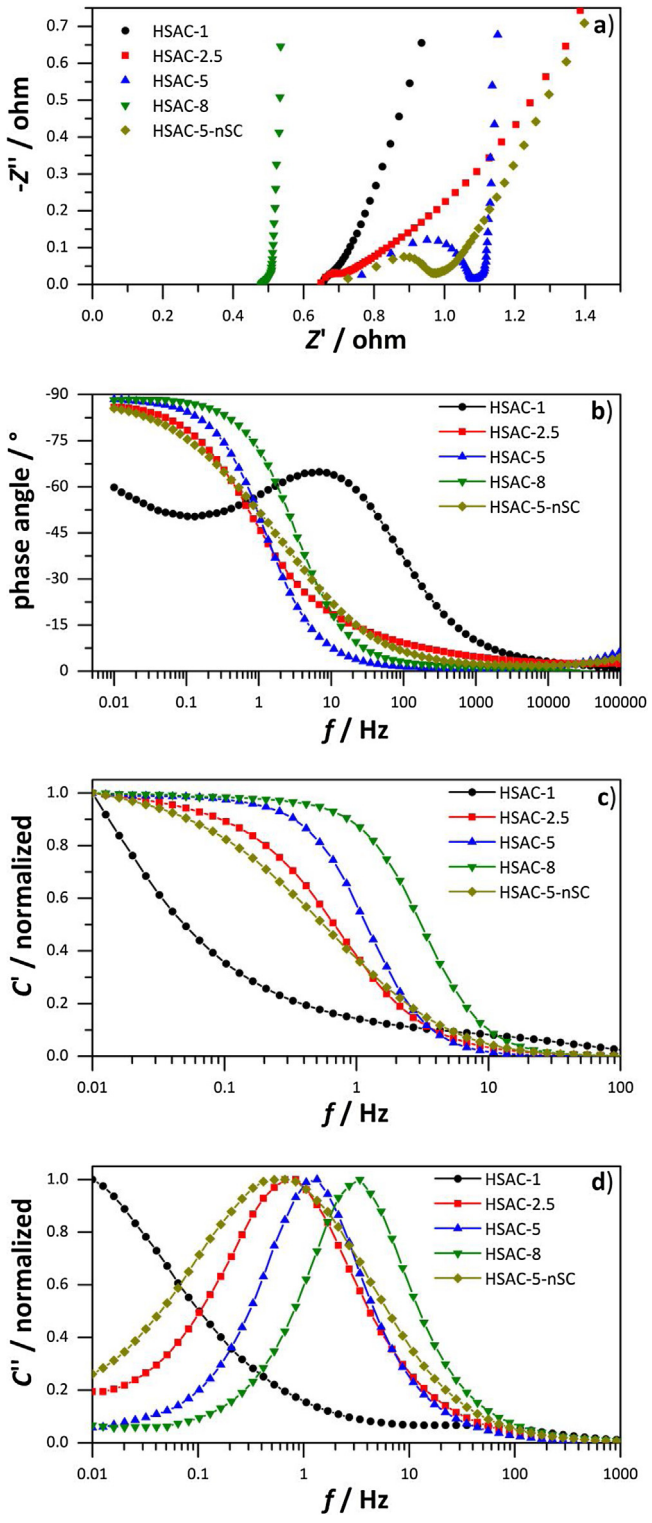

Fig. 7. (a) Nyquist-plot of the HSAC; frequency response of the (b) phase angle, (c) normalized real capacitance and (d) normalized imaginary capacitance.

larger than 50%. The time relaxation constants are >100, 1.19, 0.75, 0.29 and 1.50 s for HSAC-1, HSAC-2.5, HSAC-5, HSAC-8 and HSAC-5-nSC, respectively. All HSAC, except for HSAC-1, have very small time constants, while HSAC-8 outstands with a time constant as small as 0.29 s which is one of the smallest measured for carbons in organic electrolytes to our best knowledge. The time constant is smaller than various carbons such as carbon nanosheets [7], activated carbons from renewable sources [61,66], carbide derived Carbons

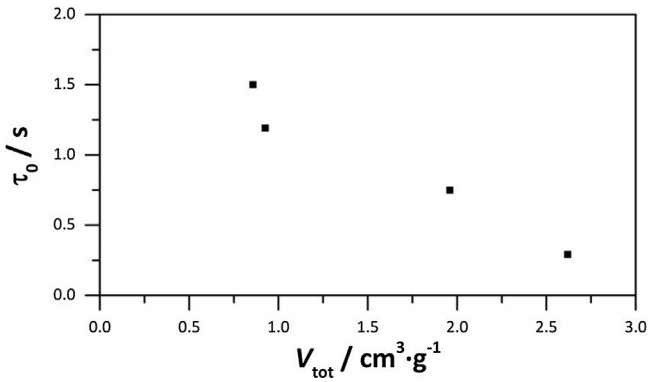

Fig. 8. Plot of the time relaxation constant τ_0 of HSAC-2.5, HSAC-5, HSAC-8 and HSAC-5-nSC against their total pore volume V_{tot}.

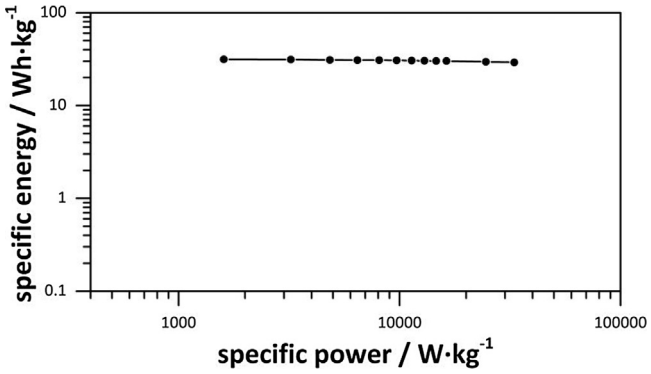

Fig. 9. Ragone plot of the fabricated capacitor based on HSAC-8 electrode material.

[9,65] graphene like carbide derived carbons [67] and commercial activated carbons [63]. Even for devices with similar electrode thickness, the time relaxation constant is significantly smaller [68]. This can be attributed to the larger mesopores, which grant fast diffusion of electrolyte ions in the pore network at higher frequencies as seen in Fig. 8. The time relaxation constant of decreases with an increasing pore volume indicating that optimization of the pore structure in carbon materials is very important to improve the overall electrochemical properties.

Whereas HSAC-5 and HSAC-8 show a good electrochemical performance with a low R_{ESR}, a short time constant and almost no loss in capacitance at high current densities, HSAC-8 exhibits the higher specific capacitance as seen in Table 2. Specific energy and power were calculated from the collected data of the galvanostatic charge/discharge experiments. As can be seen in the Ragone plot (Fig. 9) the highest specific energy of HSAC-8 is as large as 31.5 W h kg^{-1} and remains at 29.1 W h kg^{-1} up to a high power density of 33028 W kg^{-1}, which reflects the excellent retention of the capacitance with respect to high current densities. For comparison, in commercial supercapacitors the electrode material weighs about 1/3 of the whole supercapacitor, meaning that the specific energy density of HSAC-8 is still higher, than most of the commercial available supercapacitors [69–71]. HSAC-5 proves high power capability with a high specific energy of 28.4 W h kg^{-1} up to a high power density of 35439 W kg^{-1}, which is nearly as high as the specific energy of HSAC-8. The mesopores of HSAC-5 and HSAC-8 enable the electrolyte ion diffusion within the pore network at high current densities. HSAC-1, HSAC-2.5 and HSAC-5-nSC are purely microporous and their specific energy decreases with increasing current densities due to limited ion diffusion.

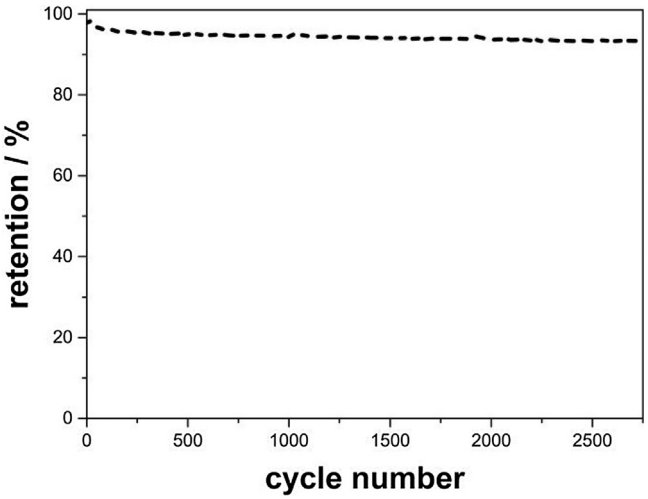

Fig. 10. Cycling stability of HSAC-8 at a current density of 2 A g^{-1}.

The long cycling life of supercapacitors is an important property and was tested for HSAC-8 with galvanostatic charge/discharge tests at 2 A g^{-1}. Fig. 10 shows the results from over 2750 cycles and HSAC-8 still Exhibits 93% of the initial capacitance indicating a good robustness of the material. The cycling stability of HSAC-8 is attributed to the double layer charge/discharge process in the electrode materials and to the mesopore content, which enables a low resistance diffusion and adsorption of electrolyte ions [52,72,73].

4. Conclusion

In summary, we have reported a novel and simple approach to produce mesoporous high surface area carbons. They were synthesized by purposely semi-carbonizing an acid catalysed PF polymer at 500 °C prior to chemical KOH activation at different KOH/carbon ratios. This way the chemical activation was more effective and carbons with large specific surface areas (up to S_{BET} ~3600 m^2 g^{-1} and S_{DFT} 2500 m^2 g^{-1}) and ultra-high total pore volumes (up to 2.6 cm^3 g^{-1}) could be produced. The semi-carbonization step was found to be crucial to obtain high surface areas as a comparison sample HSAC-5-nSC showed. Depending on the amount of KOH either purely microporous carbons or carbons with additionally mesopores up to 3.5 nm were obtained. The electrochemical performance of the HSAC heavily depends on the pore sizes, specific surface area and pore volume of the carbons. In particular, the carbons with the largest specific surface areas display the largest specific capacitance, whereupon a high content of micropores and total pore volume was found to be crucial to maximize the specific capacitance. For adequate ion diffusion within the pore network large micropores are necessary, shown in low time relaxation constants. Nevertheless, mesopores are required for a good retention of the specific capacitance with increasing current densities since larger pores offer low resistance pathways within the carbon network. Carbons like HSAC-8, with a high specific surface area, high micropore content and additional mesopores will offer supercapacitor devices with a high specific energy available at high current densities.

Acknowledgements

The authors thank Renate Walter and Dr. Frank Friedrich from the University of Hamburg for taking SEM images of the samples. The study is financed by the city of Hamburg as a part of the graduate school Keytechnologies for Sustainable Energy Systems in Smart Grids.

Appendix A. Supplementary data

Supplementary data associated with this article can be found, in the online version, at http://dx.doi.org/10.1016/j.apsusc.2017.08.095.

References

[1] A.G. Pandolfo, A.F. Hollenkamp, Carbon properties and their role in supercapacitors, J. Power Sources 157 (2006) 11–27, http://dx.doi.org/10.1016/j.jpowsour.2006.02.065.
[2] E. Frackowiak, Q. Abbas, F. Béguin, Carbon/carbon supercapacitors, J. Energy Chem. 22 (2013) 226–240, http://dx.doi.org/10.1016/S2095-4956(13)60028-5.
[3] W. Gu, G. Yushin, Review of nanostructured carbon materials for electrochemical capacitor applications: advantages and limitations of activated carbon, carbide-derived carbon, zeolite-templated carbon, carbon aerogels, carbon nanotubes, onion-like carbon, and graphene, Wiley Interdiscip. Rev. Energy Environ. 3 (2014) 424–473, http://dx.doi.org/10.1002/wene.102.
[4] Y. Zhu, S. Murali, M.D. Stoller, K.J. Ganesh, W. Cai, P.J. Ferreira, A. Pirkle, R.M. Wallace, K.A. Cychosz, M. Thommes, D. Su, E.A. Stach, R.S. Ruoff, Carbon-based supercapacitors produced by activation of graphene, Science 80 (332) (2011) 1537–1541, http://dx.doi.org/10.1126/science.1200770.
[5] Y. Zhai, Y. Dou, D. Zhao, P.F. Fulvio, R.T. Mayes, S. Dai, Carbon materials for chemical capacitive energy storage, Adv. Mater. 23 (2011) 4828–4850, http://dx.doi.org/10.1002/adma.201100984.
[6] J. Wang, H.L. Xin, D. Wang, Recent progress on mesoporous carbon materials for advanced energy conversion and storage, Part. Part. Syst. Charact. 31 (2014) 515–539, http://dx.doi.org/10.1002/ppsc.201300315.
[7] M. Sevilla, A.B. Fuertes, Direct synthesis of highly porous interconnected carbon nanosheets and their application as high-performance supercapacitors, ACS Nano 8 (2014) 5069–5078, http://dx.doi.org/10.1021/nn501124h.
[8] M. Sevilla, R. Mokaya, Energy storage applications of activated carbons: supercapacitors and hydrogen storage, Energy Environ. Sci. 7 (2014) 1250–1280, http://dx.doi.org/10.1039/c3ee43525c.
[9] B. Dyatkin, O. Gogotsi, B. Malinovskiy, Y. Zozulya, P. Simon, Y. Gogotsi, High capacitance of coarse-grained carbide derived carbon electrodes, J. Power Sources 306 (2016) 32–41, http://dx.doi.org/10.1016/j.jpowsour.2015.11.099.
[10] J. Zhou, T. Zhu, W. Xing, Z. Li, H. Shen, S. Zhuo, Activated polyaniline-based carbon nanoparticles for high performance supercapacitors, Electrochim. Acta 160 (2015) 152–159, http://dx.doi.org/10.1016/j.electacta.2015.02.032.
[11] L. Wang, J. Yu, X. Dong, X. Li, Y. Xie, S. Chen, P. Li, H. Hou, Y. Song, Three-dimensional macroporous carbon/Fe3O4 -doped porous carbon nanorods for high-performance supercapacitor, ACS Sustain. Chem. Eng. 4 (2016) 1531–1537, http://dx.doi.org/10.1021/acssuschemeng.5b01474.
[12] E. Frackowiak, Carbon materials for supercapacitor application, Phys. Chem. Chem. Phys. 9 (2007) 1774–1785, http://dx.doi.org/10.1039/b618139m.
[13] M. Inagaki, H. Konno, O. Tanaike, Carbon materials for electrochemical capacitors, J. Power Sources 195 (2010) 7880–7903, http://dx.doi.org/10.1016/j.jpowsour.2010.06.036.
[14] J. Chmiola, G. Yushin, Y. Gogotsi, C. Portet, P. Simon, P.L. Taberna, Anomalous increase in carbon capacitance at pore sizes less than 1 nanometer, Science 313 (2006) 1760–1763, http://dx.doi.org/10.1126/science.1132195.
[15] Y. Dai, H. Jiang, Y. Hu, Y. Fu, C. Li, Controlled synthesis of ultrathin hollow mesoporous carbon nanospheres for supercapacitor applications, Ind. Eng. Chem. Res. 53 (2014) 3125–3130, http://dx.doi.org/10.1021/ie403950t.
[16] N. Liu, J. Shen, D. Liu, Activated high specific surface area carbon aerogels for EDLCs, Microporous Mesoporous Mater. 167 (2013) 176–181, http://dx.doi.org/10.1016/j.micromeso.2012.09.009.
[17] Y. Meng, D. Gu, F. Zhang, Y. Shi, L. Cheng, D. Feng, Z. Wu, Z. Chen, Y. Wan, A. Stein, D. Zhao, A family of highly ordered mesoporous polymer resin and carbon structures from organic-organic self-assembly, Chem. Mater. 18 (2006) 4447–4464, http://dx.doi.org/10.1021/cm060921u.
[18] T. Cai, M. Zhou, G. Han, S. Guan, Phenol-formaldehyde carbon with ordered/disordered bimodal mesoporous structure as high-performance electrode materials for supercapacitors, J. Power Sources 241 (2013) 6–11, http://dx.doi.org/10.1016/j.jpowsour.2013.04.112.
[19] H. Teng, S.-C. Wang, Preparation of porous carbons from phenol-formaldehyde resins with chemical and physical activation, Carbon N. Y. 38 (2000) 817–824, http://dx.doi.org/10.1016/s0008-6223(99)00160-8.
[20] H. Teng, Y.-J. Chang, C.-T. Hsieh, Performance of electric double-layer capacitors using carbons prepared from phenol-formaldehyde resins by KOH etching, Carbon N. Y. 39 (2001) 1981–1987, http://dx.doi.org/10.1016/s0008-6223(01)00027-6.
[21] X. Zhang, J. Wang, Z. Yu, R. Wang, H. Xie, Highly mesoporous carbon with high capacitance from carbonization of phenol-formaldehyde resin, Mater. Lett. 63 (2009) 2523–2525, http://dx.doi.org/10.1016/j.matlet.2009.09.001.

[22] H. Chen, F. Wang, S. Tong, S. Guo, X. Pan, Porous carbon with tailored pore size for electric double layer capacitors application, Appl. Surf. Sci. 258 (2012) 6097–6102, http://dx.doi.org/10.1016/j.apsusc.2012.03.009.
[23] Z. Wang, M. Zhou, H. Chen, J. Jiang, S. Guan, Hierarchical activated mesoporous phenolic-resin-based carbons for supercapacitors, Chem.—Asian J. 9 (2014) 2789–2797, http://dx.doi.org/10.1002/asia.201402338.
[24] Y. Wang, B. Chang, D. Guan, X. Dong, Mesoporous activated carbon spheres derived from resorcinol-formaldehyde resin with high performance for supercapacitors, J. Solid State Electrochem. 19 (2015) 1783–1791, http://dx.doi.org/10.1007/s10008-015-2789-8.
[25] F. Sun, J. Gao, X. Liu, X. Pi, Y. Yang, S. Wu, Porous carbon with a large surface area and an ultrahigh carbon purity via templating carbonization coupling with KOH activation as excellent supercapacitor electrode materials, Appl. Surf. Sci. 387 (2016) 857–863, http://dx.doi.org/10.1016/j.apsusc.2016.06.176.
[26] A. Gardziella, L.A. Pilato, A. Knop, Phenolic Resins, Springer Berlin Heidelberg, Berlin, Heidelberg, 2000, http://dx.doi.org/10.1007/978-3-662-04101-7.
[27] Y. Meng, D. Gu, F. Zhang, Y. Shi, H. Yang, Z. Li, C. Yu, B. Tu, D. Zhao, Ordered mesoporous polymers and homologous carbon frameworks: amphiphilic surfactant templating and direct transformation, Angew. Chem. Int. Ed. 44 (2005) 7053–7059, http://dx.doi.org/10.1002/anie.200501561.
[28] J. Górka, M. Jaroniec, Hierarchically porous phenolic resin-based carbons obtained by block copolymer-colloidal silica templating and post-synthesis activation with carbon dioxide and water vapor, Carbon N. Y. 49 (2011) 154–160, http://dx.doi.org/10.1016/j.carbon.2010.08.055.
[29] J. Choma, K. Jedynak, W. Fahrenholz, J. Ludwinowicz, M. Jaroniec, Microporosity development in phenolic resin-based mesoporous carbons for enhancing CO2 adsorption at ambient conditions, Appl. Surf. Sci. 289 (2014) 592–600, http://dx.doi.org/10.1016/j.apsusc.2013.11.051.
[30] L.K.C. de Souza, N.P. Wickramaratne, A.S. Ello, M.J.F. Costa, C.E.F. da Costa, M. Jaroniec, Enhancement of CO2 adsorption on phenolic resin-based mesoporous carbons by KOH activation, Carbon N. Y. 65 (2013) 334–340, http://dx.doi.org/10.1016/j.carbon.2013.08.034.
[31] N.P. Wickramaratne, M. Jaroniec, Importance of small micropores in CO2 capture by phenolic resin-based activated carbon spheres, J. Mater. Chem. A. 1 (2013) 112–116, http://dx.doi.org/10.1039/C2TA00388K.
[32] Y. Yan, J. Wei, F. Zhang, Y. Meng, B. Tu, D. Zhao, The pore structure evolution and stability of mesoporous carbon FDU-15 under CO2, O2 or water vapor atmospheres, Microporous Mesoporous Mater. 113 (2008) 305–314, http://dx.doi.org/10.1016/j.micromeso.2007.11.028.
[33] X. Wang, C. Liang, S. Dai, Facile synthesis of ordered mesoporous carbons with high thermal stability by self-assembly of resorcinol-formaldehyde and block copolymers under highly acidic conditions, Langmuir 24 (2008) 7500–7505, http://dx.doi.org/10.1021/la800529v.
[34] X. Wang, J.S. Lee, C. Tsouris, D.W. DePaoli, S. Dai, Preparation of activated mesoporous carbons for electrosorption of ions from aqueous solutions, J. Mater. Chem. 20 (2010) 4602–4608, http://dx.doi.org/10.1039/b925957k.
[35] W. Xing, S.-P. Zhuo, X. Gao, Preparation of hierarchical porous carbon by post activation, Mater. Lett. 63 (2009) 1311–1313, http://dx.doi.org/10.1016/j.matlet.2009.03.008.
[36] J. Górka, A. Zawislak, J. Choma, M. Jaroniec, KOH activation of mesoporous carbons obtained by soft-templating, Carbon N. Y. 46 (2008) 1159–1161, http://dx.doi.org/10.1016/j.carbon.2008.03.024.
[37] J. Górka, A. Zawislak, J. Choma, M. Jaroniec, Adsorption and structural properties of soft-templated mesoporous carbons obtained by carbonization at different temperatures and KOH activation, Appl. Surf. Sci. 256 (2010) 5187–5190, http://dx.doi.org/10.1016/j.apsusc.2009.12.092.
[38] C. Srinivasakannan, Production of activated carbon from rubber wood sawdust, Biomass Bioenergy 27 (2004) 89–96, http://dx.doi.org/10.1016/j.biombioe.2003.11.002.
[39] Y. Liang, F. Liang, H. Zhong, Z. Li, R. Fu, D. Wu, An advanced carbonaceous porous network for high-performance organic electrolyte supercapacitors, J. Mater. Chem. A 1 (2013) 7000, http://dx.doi.org/10.1039/c3ta11051f.
[40] H. Zhong, F. Xu, Z. Li, R. Fu, D. Wu, High-energy supercapacitors based on hierarchical porous carbon with an ultrahigh ion-accessible surface area in ionic liquid electrolytes, Nanoscale 5 (2013) 4678, http://dx.doi.org/10.1039/c3nr00738c.
[41] Z. Li, D. Wu, Y. Liang, F. Xu, R. Fu, Facile fabrication of novel highly microporous carbons with superior size-selective adsorption and supercapacitance properties, Nanoscale 5 (2013) 10824–10828, http://dx.doi.org/10.1039/c3nr04236g.
[42] M. Thommes, K. Kaneko, A.V. Neimark, J.P. Olivier, F. Rodriguez-Reinoso, J. Rouquerol, K.S.W. Sing, Physisorption of gases, with special reference to the evaluation of surface area and pore size distribution (IUPAC Technical Report), Pure Appl. Chem. 87 (2015), http://dx.doi.org/10.1515/pac-2014-1117.
[43] S. Brunauer, P. Emmett, E. Teller, Adsorption of gases in multimolecular layers, J. Am. Chem. Soc. 407 (1938), http://pubs.acs.org/doi/abs/10.1021/ja01269a023 (Accessed 26 November 2012).
[44] F. Béguin, V. Presser, A. Balducci, E. Frackowiak, Carbons and electrolytes for advanced supercapacitors, Adv. Mater. 26 (2014) 2219–2251, http://dx.doi.org/10.1002/adma.201304137.
[45] G.A. Ferrero, M. Sevilla, A.B. Fuertes, Mesoporous carbons synthesized by direct carbonization of citrate salts for use as high-performance capacitors, Carbon N. Y. 88 (2015) 239–251, http://dx.doi.org/10.1016/j.carbon.2015.03.014.
[46] L. Zhang, H. Liu, M. Wang, L. Chen, Structure and electrochemical properties of resorcinol-formaldehyde polymer-based carbon for electric double-layer capacitors, Carbon N. Y. 45 (2007) 1439–1445, http://dx.doi.org/10.1016/j.carbon.2007.03.030.
[47] A.M. ElKhatat, S.A. Al-Muhtaseb, Advances in tailoring resorcinol-formaldehyde organic and carbon gels, Adv. Mater. 23 (2011) 2887–2903, http://dx.doi.org/10.1002/adma.201100283.
[48] S.-S. Tzeng, Y.-G. Chr, Evolution of microstructure and properties of phenolic resin-based carbon/carbon composites during pyrolysis, Mater. Chem. Phys. 73 (2002) 162–169, http://dx.doi.org/10.1016/S0254-0584(01)00358-3.
[49] S. Reich, C. Thomsen, Raman spectroscopy of graphite, Philos. Trans. A: Math. Phys. Eng. Sci. 362 (2004) 2271–2288, http://dx.doi.org/10.1098/rsta.2004.1454.
[50] C.-L. Liu, W.-S. Dong, J.-R. Song, L. Liu, Evolution of microstructure and properties of phenolic fibers during carbonization, Mater. Sci. Eng. A 459 (2007) 347–354, http://dx.doi.org/10.1016/j.msea.2007.02.067.
[51] A. Onodera, K. Terashima, T. Urushihara, K. Suito, H. Suimya, S. Satoh, High-pressure synthesis of diamond from phenolic resin, J. Mater. Sci. 32 (1997) 4309–4318, http://dx.doi.org/10.1023/A:1018615705312.
[52] Y. Liu, Z. Shi, Y. Gao, W. An, Z. Cao, J. Liu, Biomass-swelling assisted synthesis of hierarchical porous carbon fibers for supercapacitor electrodes, ACS Appl. Mater. Interfaces 8 (2016) 28283–28290, http://dx.doi.org/10.1021/acsami.5b11558.
[53] F. Stoeckli, T.A. Centeno, On the determination of surface areas in activated carbons, Carbon N. Y. 43 (2005) 1184–1190, http://dx.doi.org/10.1016/j.carbon.2004.12.010.
[54] T.A. Centeno, F. Stoeckli, The assessment of surface areas in porous carbons by two model-independent techniques, the DR equation and DFT, Carbon N. Y. 48 (2010) 2478–2486, http://dx.doi.org/10.1016/j.carbon.2010.03.020.
[55] P.W. Ruch, R. Kötz, A. Wokaun, Electrochemical characterization of single-walled carbon nanotubes for electrochemical double layer capacitors using non-aqueous electrolyte, Electrochim. Acta 54 (2009) 4451–4458, http://dx.doi.org/10.1016/j.electacta.2009.03.022.
[56] D. Weingarth, M. Zeiger, N. Jäckel, M. Aslan, G. Feng, V. Presser, Graphitization as a universal tool to tailor the potential-dependent capacitance of carbon supercapacitors, Adv. Energy Mater. 4 (2014), 1400316, http://dx.doi.org/10.1002/aenm.201400316.
[57] N. Jäckel, M. Rodner, A. Schreiber, J. Jeongwook, M. Zeiger, M. Aslan, D. Weingarth, V. Presser, Anomalous or regular capacitance? The influence of pore size dispersity on double-layer formation, J. Power Sources 326 (2016) 660–671, http://dx.doi.org/10.1016/j.jpowsour.2016.03.015.
[58] C. Lei, N. Amini, F. Markoulidis, P. Wilson, S. Tennison, C. Lekakou, Activated carbon from phenolic resin with controlled mesoporosity for an electric double-layer capacitor (EDLC), J. Mater. Chem. A 1 (2013) 6037, http://dx.doi.org/10.1039/c3ta01638b.
[59] Y. Xu, Z. Lin, X. Zhong, X. Huang, N.O. Weiss, Y. Huang, X. Duan, Holey graphene frameworks for highly efficient capacitive energy storage, Nat. Commun. 5 (2014) 4554, http://dx.doi.org/10.1038/ncomms5554.
[60] H. Zhang, K. Wang, X. Zhang, H. Lin, X. Sun, C. Li, Y. Ma, Self-generating graphene and porous nanocarbon composites for capacitive energy storage, J. Mater. Chem. A 3 (2015) 11277–11286, http://dx.doi.org/10.1039/c5ta01783a.
[61] M. Härmas, T. Thomberg, H. Kurig, T. Romann, A. Jänes, E. Lust, Microporous-mesoporous carbons for energy storage synthesized by activation of carbonaceous material by zinc chloride, potassium hydroxide or mixture of them, J. Power Sources 326 (2016) 624–634, http://dx.doi.org/10.1016/j.jpowsour.2016.04.038.
[62] M. Karthik, E. Redondo, E. Goikolea, V. Roddatis, S. Doppiu, R. Mysyk, Effect of mesopore ordering in otherwise similar micro/mesoporous carbons on the high-rate performance of electric double-layer capacitors, J. Phys. Chem. C 118 (2014) 27715–27720, http://dx.doi.org/10.1021/jp508581x.
[63] P.L. Taberna, P. Simon, J.F. Fauvarque, Electrochemical characteristics and impedance spectroscopy studies of carbon-carbon supercapacitors, J. Electrochem. Soc. 150 (2003) A292–A300, http://dx.doi.org/10.1149/1.1543948.
[64] Q. Wang, J. Yan, Z. Fan, Carbon materials for high volumetric performance supercapacitors: design, progress, challenges and opportunities, Energy Environ. Sci. 9 (2016) 729–762, http://dx.doi.org/10.1039/C5EE03109E.
[65] J. Segalini, B. Daffos, P.L. Taberna, Y. Gogotsi, P. Simon, Qualitative Electrochemical Impedance Spectroscopy study of ion transport into sub-nanometer carbon pores in Electrochemical Double Layer Capacitor electrodes, Electrochim. Acta 55 (2010) 7489–7494, http://dx.doi.org/10.1016/j.electacta.2010.01.003.
[66] L. Wei, M. Sevilla, A.B. Fuertes, R. Mokaya, G. Yushin, Hydrothermal carbonization of abundant renewable natural organic chemicals for high-performance supercapacitor electrodes, Adv. Energy Mater. 1 (2011) 356–361, http://dx.doi.org/10.1002/aenm.201100019.
[67] P.-C. Gao, W.-Y. Tsai, B. Daffos, P.-L. Taberna, C.R. Pérez, Y. Gogotsi, P. Simon, F. Favier, Graphene-like carbide derived carbon for high-power supercapacitors, Nano Energy 12 (2015) 197–206, http://dx.doi.org/10.1016/j.nanoen.2014.12.017.
[68] J. Zhu, Y. Xu, Y. Zhang, T. Feng, J. Wang, S. Mao, L. Xiong, Porous and high electronic conductivity nitrogen-doped nano-sheet carbon derived from polypyrrole for high-power supercapacitors, Carbon N. Y. 107 (2016) 638–645, http://dx.doi.org/10.1016/j.carbon.2016.06.063.
[69] P. Simon, A. Burke, Nanostructured carbons: double-layer capacitance and more, Electrochem. Soc. Interface 17 (2008) 38–43 http://www.scopus.com/

inward/record.url?eid=2-s2.0-77950845832&partnerID=40&md5=043ce3d463947c3fa40f034e6045ea3a.
[70] A. González, E. Goikolea, J.A. Barrena, R. Mysyk, Review on supercapacitors: technologies and materials, Renew. Sustain. Energy Rev. 58 (2016) 1189–1206, http://dx.doi.org/10.1016/j.rser.2015.12.249.
[71] A. Burke, R&D considerations for the performance and application of electrochemical capacitors, Electrochim. Acta 53 (2007) 1083–1091, http://dx.doi.org/10.1016/j.electacta.2007.01.011.
[72] T. Chou, C. Huang, R. Doong, C. Hu, Architectural design of hierarchically ordered porous carbons for high-rate electrochemical capacitors, J. Mater. Chem. A 1 (2013) 2886, http://dx.doi.org/10.1039/c2ta01190e.
[73] J. Liu, X. Wang, J. Gao, Y. Zhang, Q. Lu, M. Liu, Hollow porous carbon spheres with hierarchical nanoarchitecture for application of the high performance supercapacitors, Electrochim. Acta 211 (2016) 183–192, http://dx.doi.org/10.1016/j.electacta.2016.05.217.